Title

Calcite and dolomite formation in the CM parent body: Insight from in situ C and O isotope analyses

Authors

Telus, M
Alexander, CM O'D
Hauri, EH
et al.

Publication Date

2019-09-01

DOI

10.1016/j.gca.2019.06.012

Peer reviewed

Available online at www.sciencedirect.com

ScienceDirect

Geochimica et Cosmochimica Acta 260 (2019) 275–291

Geochimica et Cosmochimica Acta

www.elsevier.com/locate/gca

Calcite and dolomite formation in the CM parent body: Insight from *in situ* C and O isotope analyses

M. Telus *, C.M.O'D. Alexander, E.H. Hauri, J. Wang

Department of Terrestrial Magnetism, Carnegie Institution of Washington, 5241 Broad Branch Road, Washington, DC 20015, USA

Received 19 August 2018; accepted in revised form 7 June 2019; Available online 17 June 2019

Abstract

To constrain the conditions of aqueous alteration in early planetesimals, we carried out *in situ* C and O isotope analyses of calcite and dolomite and O isotope analyses of magnetite from the highly altered CM chondrites ALH 83100, ALH 84034, and MET 01070. Petrographic and isotopic analyses of these samples support previous findings of multiple generations of carbonate growth. We observe wide ranges in the C and O isotope compositions of carbonates of up to 80‰ and 30‰, respectively, that span the full range of previously reported bulk carbonate values for CM chondrites. Variations in the $\Delta^{17}O$ values indicate that fluid evolution varied for each chondrite. ALH 83100 dolomite-magnetite $\delta^{18}O$ fractionation of 23‰ ± 7‰ (2SD) corresponds to dolomite formation temperature of 125 °C ± 60 °C. $\delta^{13}C$ vs $\delta^{18}O$ values fall into two groups, one consisting of primary calcite and the other consisting of dolomite and secondary calcite. The positive correlation between $\delta^{13}C$ and $\delta^{18}O$ for primary calcite is consistent with the precipitation of calcite in equilibrium with a gas mixture of CO (or CH_4) and CO_2. The isotopic composition of calcite in CM1s and CM2s overlap significantly; however, many CM1 calcite grains are more depleted in $\delta^{18}O$ compared to CM2s. Altogether, the data indicate that the fluid composition during calcite formation was initially the same for both CM1s and CM2s. CM1s experienced more episodes of carbonate dissolution and reprecipitation where some fraction of the carbonate grains survive each episode resulting in a highly disequilibrium assemblage of carbonates on the thin-section scale.

Keywords: Carbon isotopes; oxygen isotopes; carbonates; chondrites; calcite; dolomite; meteorite; carbon; oxygen; SIMS; ion probe

1. INTRODUCTION

CM carbonaceous chondrites provide a record of progressive fluid-rock alteration in early-formed planetesimals. Although carbonates make up less than a few percent of these chondrites, they have received considerable attention because they formed via precipitation from fluids and, therefore, their formation is directly linked to the conditions of fluid alteration in the CM parent body. Calcite ($CaCO_3$) and dolomite ($CaMg(CO_3)_2$) are the most common carbonates in CM chondrites. Isotopic analyses of these phases can provide constraints on the conditions that led to the variable degrees of alteration observed in CM chondrites. Discussion of CM chondrites is complicated by the use of differing classification schemes. Some have adopted the classification scheme from Rubin et al. (2007), where the least altered CMs are classified as CM2.6s and the most altered are CM2.0s. Here, we classify the CMs on the traditional 1–3 scale for altered meteorites (Van Schmus and Wood, 1967; Zolensky et al., 1997) but using the higher resolution (1.0–2.9) petrologic assignments proposed by Alexander et al. (2013).

* Corresponding author at: Earth and Planetary Sciences, University of California Santa Cruz, 1156 High Street, Santa Cruz, CA 95064, USA.

E-mail address: mtelus@ucsc.edu (M. Telus).

https://doi.org/10.1016/j.gca.2019.06.012

0016-7037/

Bulk carbonate C and O isotopic analyses of CM chondrites exhibit a wide range of values (Clayton and Mayeda, 1984; Grady et al., 1988; Benedix et al., 2003; Guo and Eiler 2007; Alexander et al., 2015). Grady et al. (1988) and Alexander et al. (2015) analyzed the bulk $\delta^{13}C$ and $\delta^{18}O$ isotopic composition of carbonates in numerous CM chondrites, including CM1s and CM2s and falls and finds. These studies found similar ranges of values, up to 80‰ in bulk $\delta^{13}C$ values and up to 45‰ in $\delta^{18}O$ values, but Alexander et al. (2015) observed a positive correlation between $\delta^{13}C$ and $\delta^{18}O$, which is not obvious in the dataset from Grady et al. (1988). Benedix et al. (2003) analyzed the O isotopic compositions of carbonates in CM falls and found results similar to the previously mentioned studies. Clumped-isotope analyses of $\delta^{13}C$ and $\delta^{18}O$ of carbonates in CM falls (Cold Bokkeveld, Murray, and Murchison) were carried out by Guo and Eiler (2007). They observed a negative correlation in $\delta^{13}C$ vs $\delta^{18}O$ for these chondrites. These studies did not observe systematic variations between $\delta^{13}C$, $\delta^{18}O$ and petrologic type. Also, it is apparent from these studies that there can be significant variations in the bulk composition of carbonates between different aliquots of the same meteorite, indicating that averaging from bulk analyses may be obscuring important details about the isotopic record of carbonates.

In situ analyses of carbonates can provide a more detailed picture of carbonate formation from asteroidal fluids. Oxygen isotope analyses by Tyra et al. (2012) and Lee et al. (2013) revealed two morphologically, petrologically and isotopically distinct types of calcite grains in CM1 chondrites, indicating that they formed at different temperatures or possibly during discrete impact-related events on the CM parent body. Conversely, Fujiya et al. (2015) found a bimodal distribution of $\delta^{13}C$ calcite compositions in Murchison, but no differences in the O-isotopic compositions of morphologically distinct calcite grains. They suggest that the source of C for Murchison during calcite formation requires two isotopically distinct reservoirs of organic matter. More recently, Vacher et al. (2017) carried out *in situ* C and O isotope analyses of calcite in Paris, the least altered CM chondrite. They found that the range in $\delta^{13}C$ and $\delta^{18}O$ of calcite from Paris is similar to that for highly altered CMs and can potentially be explained by the contribution of soluble organic matter during equilibration of water with anhydrous rock in the CM parent body.

We carried out detailed petrology and *in situ* C and O isotope analyses of calcite and dolomite and O isotope analyses of magnetite from the highly altered CM chondrites, Alan Hills (ALH) 83100, ALH 84034, and Meteorite Hills (MET) 01070 with the aim of better understanding carbonate formation in highly altered CM chondrites. Our analyses differ from previous *in situ* studies in that the C and O isotopes were analyzed simultaneously and we also analyzed magnetite in order to try to better constrain the temperature of carbonate formation. The carbonates from these three CM1 chondrites exhibit large variations in their $\delta^{13}C$ and $\delta^{18}O$ composition that span a greater range of values than seen from bulk C and O isotope analyses of numerous CM chondrites (Alexander et al., 2015), indicating that the carbonate grains did not all form in equilibrium with the same fluid. Instead, the isotopic and petrologic evidence suggests that there were multiple episodes of carbonate formation involving incomplete dissolution of earlier generations of carbonate and reprecipitation from fluids with evolving compositions.

2. SAMPLES AND METHODS

2.1. Samples

We analyzed ALH 83100 (section 185), ALH 84034 (section 13) and MET01070 (section 45). These three CM chondrites are highly altered. Their petrology and geochemistry have been previously described (Zolensky et al., 1997; Brearley and Hutcheon, 2000; Rubin et al., 2007, Howard et al., 2015). All three have also been analyzed for bulk H, C and N, and bulk carbonate C and O isotope compositions (Alexander et al., 2013; Alexander et al., 2015). ^{53}Mn-^{53}Cr age dating has been carried out for ALH 83100 (de Leuw et al., 2009; Fujiya et al., 2012). Thin section RGB maps (Mg-Ca-Al) for all three samples are provided in the supplementary files (Figs. S1–S3). For easy comparison to the bulk C and O isotopes, we use the petrologic types from Alexander et al. (2013): ALH 83100 and ALH 84034 are type 1.1 and MET 01070 is a type 1.2 based on bulk H content (or 2.1, 2.1, and 2.0 respectively using the classification described by Rubin et al., 2007). These classifications are also consistent with those determined from modal mineralogy analyses (Howard et al., 2015).

2.2. Petrology

For each thin section, we collected reflected light maps using a Nikon optical microscope, and elemental maps (1 nA, 15 kV) using Carnegie's JEOL 6500 scanning electron microscope (SEM), which is equipped with an Oxford XMaxN 80 mm^2 large area silicon drift EDS detector. These maps were used to identify Ca-carbonate and magnetite grains for ion probe analyses. We also used Carnegie's JEOL 8530F electron probe for cathodoluminescence (CL) mapping of carbonate grains (20 nA, 20 kV, 20 ms dwell time). The C coatings, used for the SEM analyses, were removed and replaced with Au coatings prior to ion probe analyses.

2.3. In situ isotope analyses

In situ C and O isotope analyses of carbonates and O isotope analyses of magnetite were carried out using Carnegie's NanoSIMS 50L with a Cs^+ primary beam of ~70–100 pA. Negative ions of $^{12}C^-$, $^{13}C^-$, $^{17}O^-$, and $^{18}O^-$ were measured with electron multipliers (EMs), while $^{16}O^-$ was measured with a Faraday cup. The electron gun was used for charge compensation. A mass resolving power of 9000 was used to separate interferences from the peaks of interest (e.g., $^{16}OH^-$ from $^{17}O^-$). For each measurement, the primary beam was rastered over 5 × 5 μm for presputtering, then reduced to 3 × 3 μm for the analysis. Real-time images were checked before and after each analysis to ensure that cracks or multiple phases were not included in the analyzed

areas. For ALH 84034, we analyzed 9 calcite, 10 dolomite, and 5 magnetite grains. We analyzed 12 calcite, 11 dolomite and 5 magnetite grains from ALH 83100. For MET 01070, we analyzed 40 calcite grains and 4 dolomite grains, but no magnetite grains as most were too small for SIMS analyses. Sample-standard bracketing with terrestrial calcite (USNM 136321), dolomite (USNM 10057) and magnetite (Charoy) standards was used to correct for drift in the yields of the electron multipliers and instrumental mass fractionation (IMF). The variation in the standard $\delta^{13}C$ and $\delta^{18}O$ isotopic compositions are ±1.5‰ and ±0.9‰ (2SD), respectively, for calcite, ±0.6‰ and ±1.5‰ (2SD), respectively, for dolomite and ± 2.7‰ (2SD) for $\delta^{18}O$ in magnetite. The C and O isotope composition of standards analyzed during ALH 84034 dolomite analyses are provided in the supplementary files (Table S4). The uncertainties in the isotope ratios include errors from the IMF corrections and counting statistics. Delta values were calculated relative to Standard Mean Ocean Water (SMOW) for O isotopes, and relative to Pee-Dee Belemnite (PDB) for C isotopes. Throughout the text, 2σ uncertainties are reported, unless stated otherwise. After isotope analyses, all spots were checked in the SEM to ensure that the target areas were indeed analyzed.

2.4. Evaluating possible matrix-effects

Matrix-matched standards are important for SIMS analyses, but they are often difficult to acquire, especially for meteorite analyses. Bias in SIMS data from matrix-effects arise from differences in the instrumental mass fractionation that is related to mineral composition. Matrix-effects have been shown to increase with increasing Fe and Mn content in carbonates (Sliwinski et al., 2015a, b; Rollion-Bard and Marin-Carbonne, 2011).

The carbonate standards used for our analyses, calcite (USNM 136321) and dolomite (USNM 10057), do not have Fe (Jarosewich and MacIntyre, 1983). The average Fe content in CM calcite from MET 01070, ALH 83100 and ALH 84034 is 0.32 wt.%, 0.31 wt.% and 0.81 wt.%, respectively. The average Fe content of CM dolomite is 2.39 wt.% and 3.67 wt.% for ALH 83100 and ALH 84034, respectively. Average Mn and Mg content of calcite in the CM chondrites analyzed for this study are negligible. The SEM EDS compositional data is summarized in the supplementary files (Table S5).

Based on work by Rollion-Bard and Marin-Carbonne (2011), the O-isotope analyses of CM calcite from this study, which has <1 wt% FeO and MnO, should not be significantly affected by matrix-effects (i.e., the bias should be <±1‰). We assume that the C isotope analyses of calcite are similarly unaffected with such low Fe and Mn contents. The CM dolomite have little Mn, but the Fe content of 2.4–3.7 wt% could potentially result in significant matrix-effects. Based on Sliwinski et al. (2015a,b) the average Fe# of approximately 0.1 for CM carbonates could produce significant bias of −2.5‰ and +5.5‰ for $\delta^{13}C$ and $\delta^{18}O$, respectively.

Although, we cannot simply use the Sliwinski et al., studies to correct our data because the instrumental conditions differ significantly, we use them to evaluate the potential magnitude of bias from matrix-effects and how this may influence the results. Given that the potential bias is likely <10‰, we can correct for matrix-effect by subtracting the bias from the measured ratio, $\delta R_{true} = \delta R_{measured} - \delta R_{bias}$, where R refers to $\delta^{13}C$ or $\delta^{18}O$ and the measured ratio, $\delta R_{measured}$, has already been corrected for IMF and drift (Kita et al., 2009).

Overall, the compositions of the CM calcite grains are similar enough to the calcite standard that a matrix-correction is not necessary for calcite. On the other hand, the Fe content of CM dolomite is significantly different from the standard. We evaluate potential bias in the dolomite data by applying corrections of −2.5‰ for $\delta^{13}C$, +2.9‰ and +5.5‰ for $\delta^{17}O$ and $\delta^{18}O$, respectively.

Below, both matrix-corrected and -uncorrected C and O isotope data are shown for comparison (only the dolomite values change), but these corrections do not change our interpretation; therefore, only the uncorrected data are discussed in the results and discussion sections.

3. RESULTS

3.1. Occurrence of carbonates and magnetite in CM1s

Figs. 1–3 show examples of grains that were analyzed for this study from ALH 83100, ALH 84034, and MET 01070, respectively. Backscatter (BSE) images and/or elemental maps for many of the analyzed grains are provided in supplementary files (Fig. S6). Dolomite and calcite are abundant in ALH 83100 and ALH 84034, and present in approximately equal proportions. They mainly occur in the matrix, but were also observed along chondrule rims and within chondrule pseudomorphs. Large (>10 μm) dolomite grains are abundant in both ALH samples. They occur as single isolated grains or along the peripheries of calcite grains. For ALH 84034, the dolomite grains are smooth in texture (e.g., Fig. 2C), while those in ALH 83100 have considerably more pits (e.g., Fig. 1a). MET 01070 carbonate grains occur mainly in the matrix, though some are associated with chondrules. The calcite grains are largely free of mineral inclusions and the sizes vary from less than 5 μm to ~100 μm across. We analyzed only a few dolomite grains in MET 01070 because most are too small (<3 μm) for SIMS analyses. The thin section contains several regions with abundant fine-grained calcite and dolomite. These can be seen in the thin section maps provided in the supplementary material (Fig. S1). Dolomite occurs on the periphery of calcite grains, even in the fine-grained mixtures.

Calcite grains in all the samples mainly occur as anhedral, inclusion-free grains. These are classified as type 1 (Tyra et al., 2012; Lee et al., 2014). Calcite can occur as inclusions within dolomite grains. These calcite grains also appear to be type 1 grains. Type 2 calcite grains are characterized by their mottled texture (Tyra et al., 2012; Lee et al., 2014). MET 01070 has a few type 2 calcite, but there are no obvious type 2 calcite grains in our sections of the two ALH meteorites.

Magnetite is rare in all three samples. Subhedral magnetite grains are dispersed sporadically in the matrix and

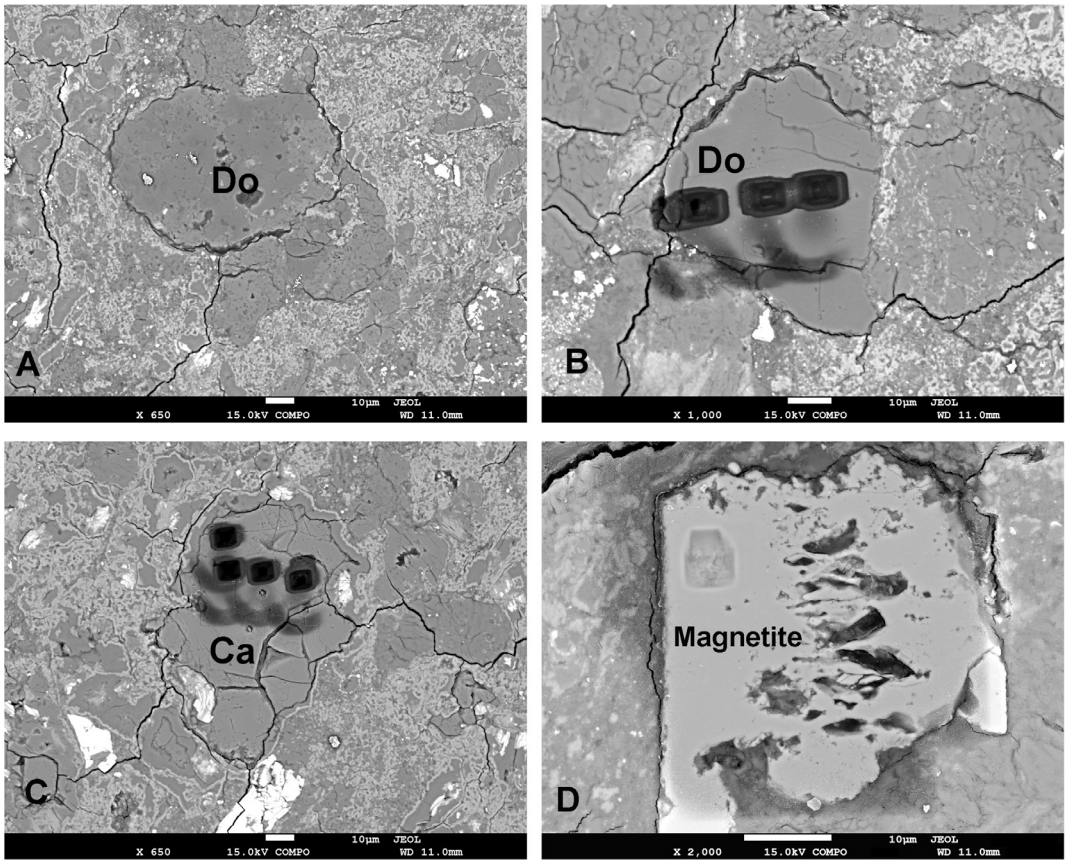

Fig. 1. Backscatter electron (BSE) images of dolomite (Do), calcite (Ca), and magnetite grains in ALH 83100. The dark pits are from NanoSIMS analyses.

rims of chondrule pseudomorphs in the ALH samples (Figs. 1 and 2). They are often pitted and/or have inclusions filled with Fe-rich phyllosilicates. Previous analyses have found that magnetite abundances increase with increasing aqueous alteration, possibly as a result of oxidation of Fe-Ni metal and/or the breakdown of Fe-crondstedtite (Rubin et al., 2007; Howard et al., 2015; King et al., 2017). Sample "Mgt 1" from ALH 83100 was the only analysis associated with framboidal magnetite. We did not observe intergrowths that could be used to determine if magnetite formed before, at the same time as, or after carbonates. The examples shown in Figs. 1d and 2d exhibit sharp contacts with the surrounding matrix. We observed only a few magnetite grains in MET 01070, most occur within a single chondrule pseudomorph.

3.2. Calcite cathodoluminescence spectra

Cathodoluminescence (CL) spectra were collected for most of the calcite grains. There are two main CL peaks for calcite at ~375 nm and 610 nm (Fig. 4), which are controlled by the relative abundance of Mn^{2+} and Fe^{2+}. The presence of Mn in calcite activates CL, while Fe quenches it. In general, calcite with high Mn/Fe ratios are strongly luminescent, those with low Mn/Fe ratios have dull luminescence, and those with <100 ppm Mn and <200 ppm Fe are nonluminescent (Barnaby and Rimstidt, 1989). It is not completely clear why some calcite have red CL (600 nm), while others appear blue (375 nm), but it is likely related to high Mn content and intrinsic CL, respectively (Boggs and Krinsley, 2006; Richter et al., 2003). A large area CL map of MET 01070 is available in the supplementary files (Fig. S7).

CL for calcite in MET 01070 reveals two distinct groups of calcite grains, those with relatively small peaks at 610 nm (<20 counts) and those with large peaks at 610 nm (>20 counts). Calcite grains from ALH 83100 and ALH 84034 show little variation in the intensity of the CL peaks and all have relatively small 610 nm peaks and large 375 nm peaks. Since CL in calcite is predominately activated by Mn^{2+} impurities in the crystal lattice, we refer to the two groups of calcite in MET 01070 as Mn-poor (those with 610 nm peaks with <20 counts) or Mn-rich (those with 610 nm peaks >20 counts). The Mn-poor calcite grains have MnO contents that are below the detection limit of the SEM (<0.1 wt.%) and the Mn-rich grains have MnO contents of 1–1.5 wt.%. Dolomite in MET 01070 is only associated with the Mn-rich calcite grains.

The CL maps shown in Fig. 5 provide petrographic context for the two groups of calcite grains in MET 01070. They show that the Mn-rich grains (red in the CL map) are anhedral in shape and occur on the periphery of

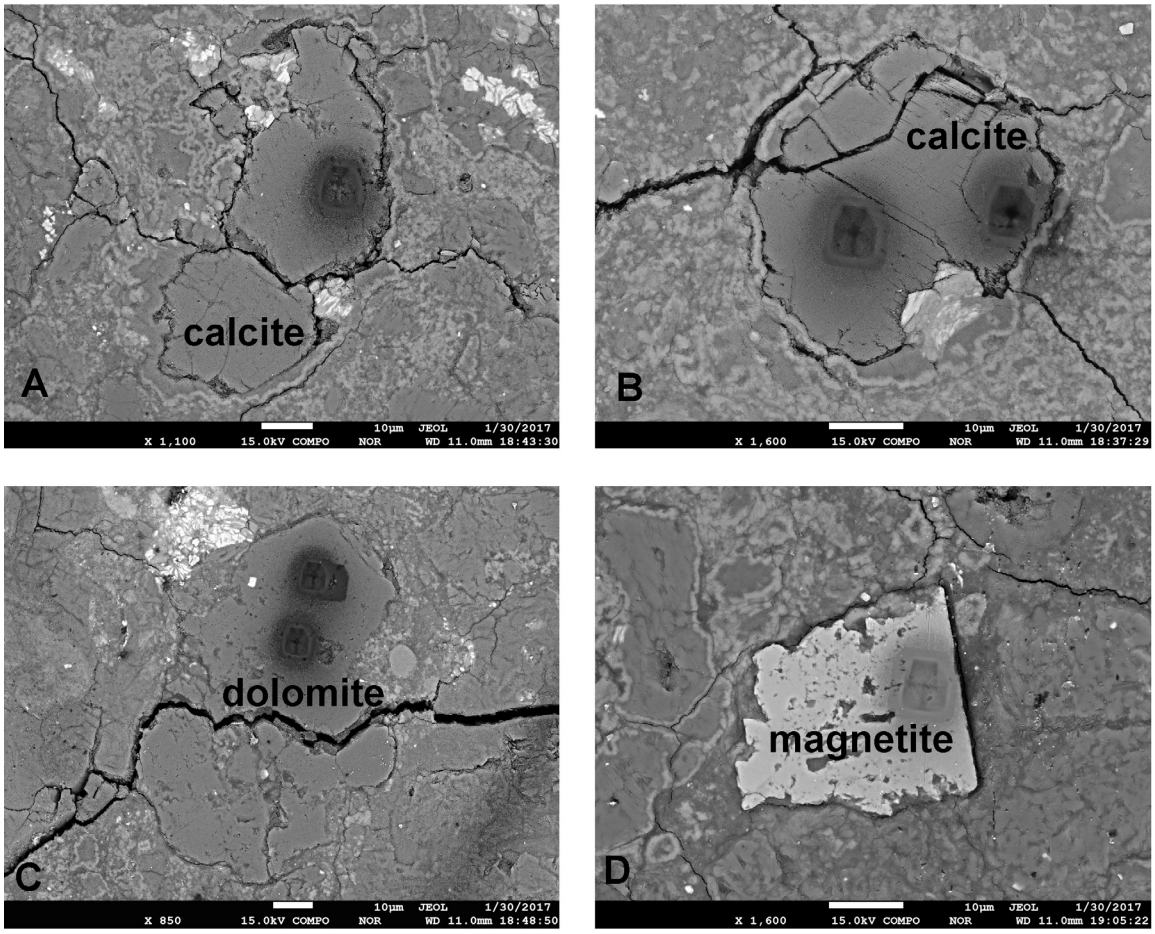

Fig. 2. BSE images of calcite, dolomite and magnetite grains in ALH 84034. The dark pits are from the NanoSIMS analyses.

Mn-poor grains (blue in the CL map), which are often euhedral/subhedral in shape. We often refer to the Mn-rich grains as "secondary" and the Mn-poor grains as "primary" based on their petrologic relationship. The red wavelength is 610 nm and the blue is 375 nm. Fig. 5 also includes 500 nm wavelength in green because it appears to show some alteration within the calcite grains (disregard green CL signature from the epoxy in the fracture in the thin section).

CL can be used to distinguish between calcite and aragonite, which have the same major element chemical compositions, but different crystal structures. All of the samples we analyzed have CL peaks at 375 nm, which is characteristic of calcite but not aragonite. Aragonite has a single peak at 550–580 nm (Boggs and Krinsley, 2006).

3.3. In situ O isotope compositions of carbonate and magnetite

These highly altered chondrites exhibit large variations in their carbonate and magnetite O-isotope compositions on small spatial scales. The O-isotopic compositions and the $\Delta^{17}O$ values are summarized in Table 1 and shown in Fig. 6A and 7, respectively. The O-isotope compositions of the carbonate and magnetite grains in ALH 83100 scatter around the terrestrial mass fractionation line (TFL), with $\Delta^{17}O$ values for calcite from −2‰ to +4‰, −3‰ to +3‰ for dolomite and 0‰ to +3‰ for magnetite. Despite the limited range of $\Delta^{17}O$ values, there is a considerable range in mass fractionations. The $\delta^{18}O$ values of calcite grains range from +14‰ to +40‰. Dolomite grains are systematically less fractionated compared to calcite with $\delta^{18}O$ values ranging from +20‰ to +24‰. The $\delta^{18}O$ values for magnetite range from −15‰ to +4‰. The framboidal magnetite grain is depleted in $\delta^{18}O$ (−15‰) compared to the isolated magnetite grains, which have an average composition of −0.8‰.

For ALH 84034, calcite and dolomite have similar ranges of O-isotopic compositions. The $\Delta^{17}O$ values range from −9‰ to +5‰ for calcite, −6‰ to +7‰ for dolomite and −9‰ to −2‰ for magnetite. The result is a trend with a slightly steeper slope than the TFL. The calcite grains have a more restricted range of $\delta^{18}O$ values (+12‰ to +28‰) than in ALH 83100, but the dolomite grains show more variation (+7‰ to +22‰) than in ALH 83100. The O-isotopic compositions of the magnetite exhibit a similar range in $\delta^{18}O$ (−14‰ to −1‰) to those in ALH 83100.

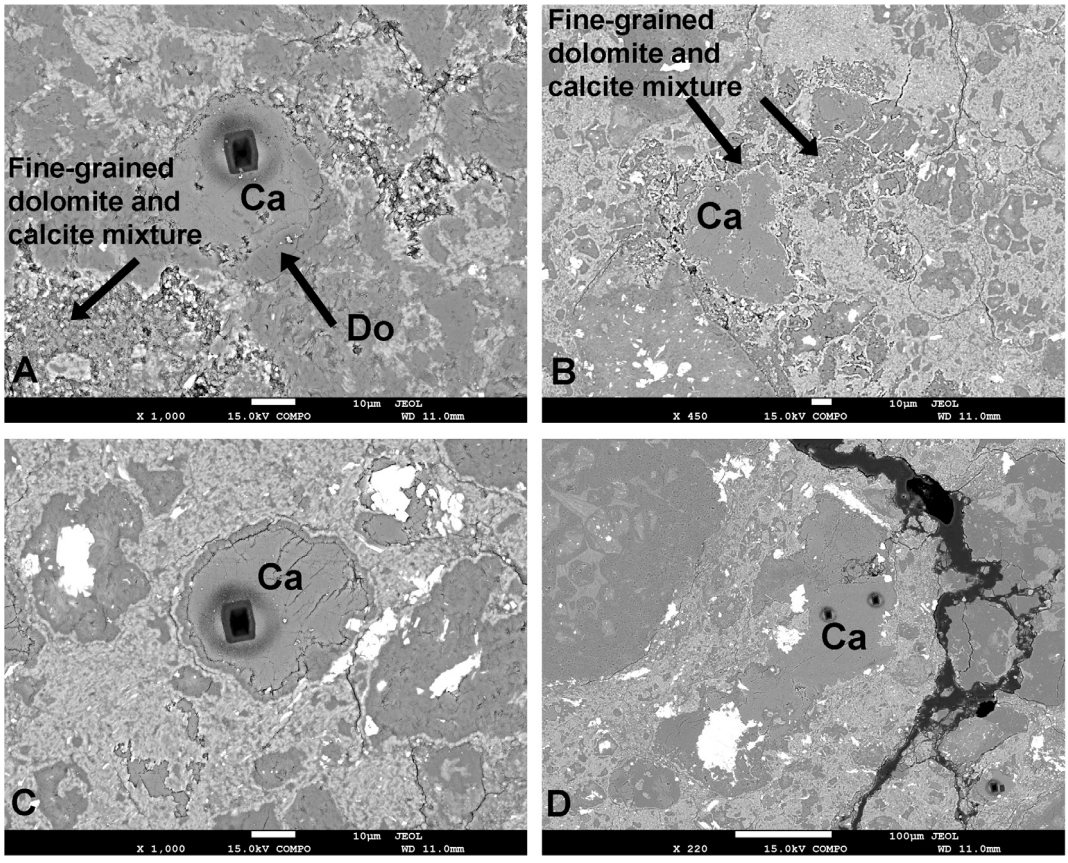

Fig. 3. BSE images of dolomite (Do) and calcite (Ca) grains in MET 01070. Fine-grained mixtures of calcite and dolomite occur over large areas (>1 mm^2) of this thin section. The dark pits are from the NanoSIMS analyses.

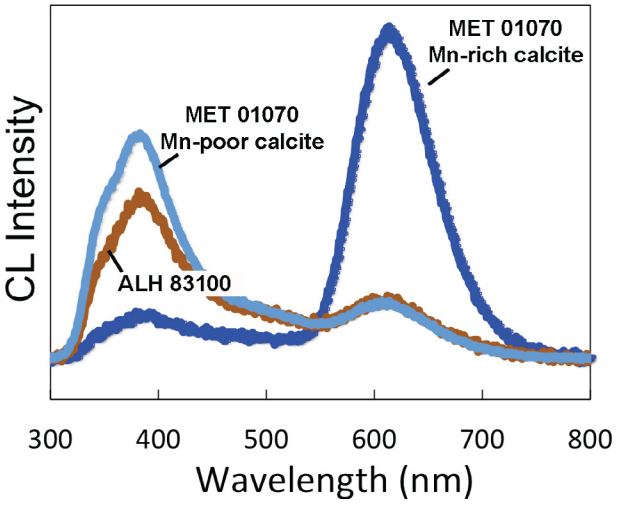

Fig. 4. Cathodoluminescence (CL) spectra for calcite from MET 01070 shows two types of calcite grains: Those with relatively small peaks at 610 nm and large peaks at 375 nm (light blue), and those with large peaks at 610 nm and small peaks at 375 nm (dark blue). CL spectra for ALH 83100 (orange) and ALH 84034 (not shown) do not have large peaks at 610 nm. (For interpretation of the references to color in this figure legend, the reader is referred to the web version of this article.)

The two groups of calcite grains in MET 01070 have similar ranges of $\Delta^{17}O$ values, with average values of −4‰ and −5‰ for Mn-poor and Mn-rich calcite, respectively. However, Mn-poor grains have mean $\delta^{18}O$ compositions of 38 ± 8‰, while the $\delta^{18}O$ of Mn-rich grains are 25 ± 3‰. The dolomite analyses were few (n = 4) because most grains were too small. Those that could be analyzed exhibit a similar range in $\Delta^{17}O$ values to the calcite grains but have an average $\delta^{18}O$ of 16‰.

The $\Delta^{17}O$ vs. $\delta^{18}O$ values for calcite, dolomite and magnetite for each chondrite are shown in Fig. 7. The $\Delta^{17}O$ values of the carbonates and the magnetite in ALH 84034 differ by ~6‰, while there is no difference in $\Delta^{17}O$ values for carbonates and magnetite from ALH 83100. The $\Delta^{17}O$ values for MET 01070 are lower than those for ALH 84034 and ALH 83100. The Mn-rich secondary calcites have slightly lower $\Delta^{17}O$ values than the Mn-poor primary calcite grains, though this difference is not statistically significant.

There is no significant change to the results when matrix-corrections are applied to dolomite (see Section 2.4 for details). The matrix-effect-corrected O-isotope values for dolomite are plotted for comparison (Fig. 6B). If these corrections are applied to the dolomite data, the O isotope values for dolomite simply shift down the slope-1 line by a few permil.

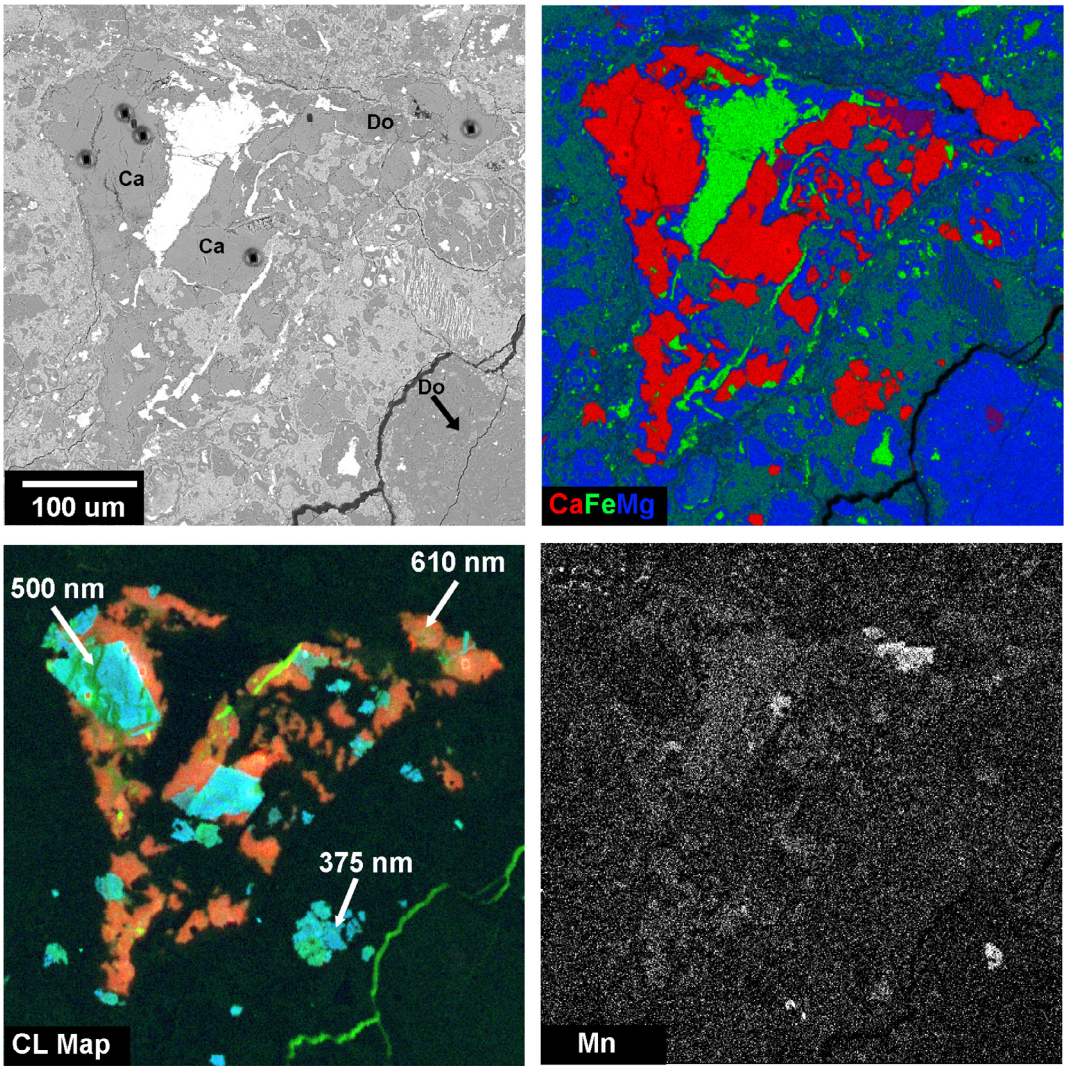

Fig. 5. BSE, CaFeMg, CL, and Mn map of calcite (Ca) from MET 01070 analyzed by SIMS for this study. The CL map is an RGB map with the 610 nm peak in red, the 500 nm peak in green and the 375 nm peak in blue. Manganese-rich calcite grains (red in CL map) occur on the periphery of Mn-poor calcite grains (blue in CL map). Dolomite (Do) grains are small and always associated with the Mn-rich calcite. The 500 nm data in green appears to show some alteration within the calcite grains (disregard green CL signature from the epoxy within the fracture in the thin section). A large area CL map of MET 01070 is available in the supplementary files. (For interpretation of the references to color in this figure legend, the reader is referred to the web version of this article.)

3.4. $\delta^{13}C$ vs. $\delta^{18}O$ of calcite and dolomite

The $\delta^{13}C$ and $\delta^{18}O$ values of the carbonate grains in the three meteorites span a greater range than that reported for the bulk carbonate compositions of 64 CM chondrites (Alexander et al., 2015). The data is provided in Table 1. In the plot of $\delta^{13}C$ vs. $\delta^{18}O$ (Fig. 8A), dolomite grains in the ALH samples have systematically higher $\delta^{13}C$ values than calcite. Their $\delta^{18}O$ values overlap significantly with calcite, but the dolomite grains tend toward lower values. The calcite and dolomite grains in ALH 84034 have relatively homogenous $\delta^{13}C$ values, ~27‰ and ~53‰, respectively, but show a range in $\delta^{18}O$ compositions. The $\delta^{13}C$ values for calcite in ALH 83100 range from 10 to 30‰, but most have values of ~25‰, consistent with most calcite grains from ALH 84034. Dolomite in ALH 83100 is relatively homogeneous in both C and O isotopes. The calcite in MET 01070 is more enriched in ^{13}C and ^{18}O than in the other two meteorites. The calcite grains plot in two groups, the Mn-poor calcite have low $\delta^{13}C$ and high $\delta^{18}O$ values, while the Mn-rich calcite have high $\delta^{13}C$ and low $\delta^{18}O$ values. It is not clear why there are a few Mn-poor grains that plot with the Mn-rich ones, but these particular grains are quite small and the CL signal for these may be biased by edge effects from the SIMS pit. Dolomite in MET 01070 have similar $\delta^{13}C$ signatures as Mn-poor calcite, but is depleted in ^{18}O. Relative to Mn-rich calcite grains, dolomite have similar $\delta^{18}O$ composition, but are depleted in ^{13}C. Overall, the data fall into two groups on a $\delta^{13}C$ vs. $\delta^{18}O$ plot. One group has relatively low $\delta^{13}C$ and high $\delta^{18}O$ values and consists of Mn-poor calcite from MET 01070 and calcite from ALH 83100 and ALH 84034.

Table 1
C and O isotope composition of calcite, dolomite, and magnetite in CM1 chondrites 2σ uncertainties are reported here.

ALH 84034						
Calcite						
		$\delta^{13}C$	$\delta^{17}O$	$\delta^{18}O$	$\Delta^{17}O$	
	ALH ×1 c	26.8 ± 1.4	3.6 ± 0.8	14.7 ± 0.7	−4.0 ± 1.1	
	ALH ×4 c	23.4 ± 1.4	3.1 ± 0.8	11.9 ± 0.7	−3.1 ± 1.1	
	ALH ×6 c	30.0 ± 1.5	2.5 ± 0.8	21.7 ± 0.7	−8.7 ± 1.1	
	ALH ×10 c	25.7 ± 1.3	13.6 ± 1.0	20.9 ± 1.5	2.7 ± 1.8	
	ALH ×13 c	27.2 ± 1.3	13.2 ± 1.0	24.7 ± 1.5	0.4 ± 1.8	
	ALH ×15 c	27.0 ± 1.9	19.4 ± 2.5	28.1 ± 0.5	4.8 ± 2.5	
	ALH ×17 c	28.8 ± 1.9	13.0 ± 2.5	24.4 ± 0.5	0.3 ± 2.5	
	ALH R1c	27.1 ± 0.7	6.2 ± 1.4	12.2 ± 0.2	−0.2 ± 1.2	
	ALH ×8 c	27.9 ± 0.3	14.2 ± 2.3	22.6 ± 0.6	2.4 ± 2.1	
Dolomite						
	ALH ×11 d	56.0 ± 0.9	17.7 ± 1.1	20.7 ± 0.6	6.9 ± 1.2	No calcite
	ALH ×12 d	53.5 ± 0.9	17.0 ± 1.1	21.9 ± 0.6	5.6 ± 1.2	No calcite
	ALH ×14 d	56.2 ± 1.2	11.6 ± 0.9	17.3 ± 2.5	2.5 ± 2.7	No calcite
	× 27 d	53.5 ± 1.3	9.8 ± 0.9	22.1 ± 3.1	−1.6 ± 3.2	No calcite
	ALH ×3	48.6 ± 4.5	3.1 ± 0.9	8.6 ± 0.7	−1.4 ± 0.5	No calcite
	ALH ×9	54.7 ± 0.1	14.7 ± 0.2	16.6 ± 1.3	6.1 ± 0.9	No calcite
	ALH ×2 c	50.0 ± 1.4	−2.6 ± 0.8	7.0 ± 0.7	−6.2 ± 1.1	Calcite
	ALH ×5	52.0 ± 4.9	2.3 ± 0.4	8.1 ± 0.2	−2.0 ± 0.5	Calcite
	ALH ×7 d	54.0 ± 0.9	10.4 ± 1.1	17.7 ± 0.6	1.2 ± 1.2	∼1 μm cal. inclusions
	ALH × 16 d	52.8 ± 1.1	9.8 ± 0.8	12.2 ± 2.5	3.4 ± 2.7	∼1 μm cal. inclusions
Magnetite						
	× 22 mgt		−6.7 ± 2.8	−8.4 ± 3.1	−2.4 ± 4.2	
	× 23 mgt		−9.7 ± 2.8	−1.0 ± 3.1	−9.2 ± 4.2	
	× 25 mgt		−9.2 ± 3.4	−9.7 ± 1.9	−4.1 ± 3.9	
	×18 avg		−15.8 ± 4.4	−13.6 ± 6.5	−8.8 ± 1.0	
	×24		−12.5 ± 1.7	−14.1 ± 2.2	−5.2 ± 1.5	
ALH 83100						
Calcite						
		$\delta^{13}C$	$\delta^{17}O$	$\delta^{18}O$	$\Delta^{17}O$	
	ALH CC1 CC2	30.6 ± 2.3	20.3 ± 1.5	36.5 ± 3.3	1.3 ± 3.6	
	ALH CM	25.7 ± 1.6	19.4 ± 1.1	33.3 ± 2.3	2.1 ± 2.5	
	ALH CMt	29.3 ± 1.6	24.3 ± 1.1	40.2 ± 2.3	3.4 ± 2.5	
	ALHCB	13.6 ± 1.7	9.1 ± 0.5	14.3 ± 2.9	1.6 ± 2.9	
	ALH CA	9.4 ± 4.5	7.1 ± 0.7	15.5 ± 2.9	−1.0 ± 3.0	
	ALHCN	20.8 ± 2.2	12.0 ± 0.9	26.1 ± 1.9	−1.5 ± 2.1	
	ALHCNt	23.0 ± 2.2	14.8 ± 0.9	30.8 ± 1.9	−1.3 ± 2.1	
	ALHCNt5	22.1 ± 2.2	16.8 ± 0.9	32.5 ± 1.9	−0.1 ± 2.1	
	ALHDKc1	27.8 ± 3.2	16.3 ± 0.8	26.7 ± 2.6	2.4 ± 2.7	
	ALHDKc2	28.2 ± 3.2	14.6 ± 0.8	20.7 ± 2.6	3.8 ± 2.7	
	ALHCC010302	23.4 ± 1.1	15.1 ± 1.1	33.2 ± 2.7	−2.1 ± 2.9	
	ALHCC010304	21.7 ± 1.1	16.2 ± 1.1	35.6 ± 2.7	−2.3 ± 2.9	
Dolomite						
	ALH Do	46.8 ± 0.1	8.7 ± 0.3	21.6 ± 0.6	−2.6 ± 0.7	
	ALHCNDt	49.2 ± 0.9	11.2 ± 0.4	21.8 ± 0.8	−0.1 ± 0.9	
	ALHCNDt2	39.2 ± 0.9	11.4 ± 0.4	21.0 ± 0.8	0.4 ± 0.9	
	ALHCNt3	45.0 ± 0.9	12.6 ± 0.4	23.8 ± 0.8	0.2 ± 0.9	
	ALHCNt4	46.4 ± 0.9	12.7 ± 0.4	23.4 ± 0.8	0.5 ± 0.9	
	ALHDI	48.3 ± 0.9	12.9 ± 0.9	20.3 ± 1.8	2.3 ± 2.1	
	ALHDo010303	50.6 ± 0.8	11.9 ± 0.9	20.1 ± 1.2	1.5 ± 1.5	
	ALHDo010306	57.6 ± 0.8	13.8 ± 0.9	21.8 ± 1.2	2.4 ± 1.5	
	ALHDo010307	47.4 ± 0.8	14.9 ± 0.9	23.0 ± 1.2	3.0 ± 1.5	
	ALHDo010308	54.0 ± 0.8	15.0 ± 0.9	22.3 ± 1.2	3.5 ± 1.5	
	ALHDA	51.1 ± 9.8	9.4 ± 1.0	22.7 ± 5.1	−2.4 ± 5.2	
Magnetite						
	mgt3		0.8 ± 2.7	−1.5 ± 2.8	1.6 ± 3.9	
	mgt4		4.2 ± 2.7	3.8 ± 2.8	2.2 ± 3.9	

(*continued on next page*)

Table 1 (*continued*)

ALH 83100						
	mgt5		0.7 ± 2.7	−1.0 ± 2.8	1.2 ± 3.9	
	mgt6		0.6 ± 2.7	−4.7 ± 2.8	3.1 ± 3.9	
	mgt1*		−7.7 ± 6.7	−15.1 ± 1.6	0.1 ± 6.9	
MET 01070						
		CL spectral features				
Calcite Mn-rich	375 nm	610 nm	$\delta^{13}C$	$\delta^{17}O$	$\delta^{18}O$	$\Delta^{17}O$
	META3	7	34	61.4 ± 1.4	10.1 ± 1.8	28.4 ± 2.1	−4.7 ± 2.8
	META4	5	41	64.2 ± 1.4	11.4 ± 1.8	25.7 ± 2.1	−2.0 ± 2.8
	MET_A05	5	40	60.8 ± 0.5	6.5 ± 1.4	28.1 ± 1.5	−8.1 ± 2.0
	MET A3, A01	7	41	62.6 ± 1.5	6.9 ± 2.3	25.6 ± 2.6	−6.4 ± 3.4
	META9	2	72	67.8 ± 2.1	6.7 ± 1.8	21.9 ± 2.1	−4.7 ± 2.8
	XK A10 A11	5	68	65.6 ± 2.9	9.3 ± 2.6	19.5 ± 3.0	−0.9 ± 3.9
	META14	2	70	69.6 ± 2.1	10.1 ± 1.8	25.2 ± 2.1	−3.0 ± 2.8
	META16	3	66	78.7 ± 2.1	8.3 ± 1.8	23.2 ± 2.1	−3.7 ± 2.8
	MET_D02	4	50	65.1 ± 1.4	4.6 ± 0.6	21.9 ± 1.5	−6.8 ± 1.6
	MET_E01	7	48	58.5 ± 1.4	3.8 ± 3.5	26.1 ± 1.9	−9.8 ± 4.0
	MET_E02	4	31	50.3 ± 1.4	7.3 ± 3.5	28.9 ± 1.9	−7.7 ± 4.0
	MET_E04	5	31	64.5 ± 1.4	5.0 ± 3.5	27.1 ± 1.9	−9.1 ± 4.0
	MET_E05	6	42	66.6 ± 1.4	9.3 ± 3.5	28.7 ± 1.9	−5.6 ± 4.0
	MET_G03	13	104	58.0 ± 1.4	5.0 ± 0.7	18.7 ± 1.3	−4.7 ± 1.5
	MET_H01	10	68	82.0 ± 2.0	14.6 ± 3.0	28.8 ± 3.8	−0.4 ± 4.9
	MET_B06	6	46	64.5 ± 1.4	4.6 ± 0.6	22.4 ± 1.5	−7.0 ± 1.6
Calcite Mn-poor						
	META5	28	7	30.3 ± 1.4	20.3 ± 1.8	40.0 ± 2.1	−0.5 ± 2.8
	MET A1, A2	29	8	33.8 ± 2.0	21.6 ± 3.4	43.1 ± 0.6	−0.8 ± 3.5
	META8	17	11	29.1 ± 2.1	15.8 ± 1.8	31.4 ± 2.1	−0.5 ± 2.8
	META12	12	9	49.7 ± 2.1	13.8 ± 1.8	40.3 ± 2.1	−7.2 ± 2.8
	META15	10	11	42.9 ± 2.2	19.7 ± 1.8	40.6 ± 2.1	−1.4 ± 2.8
	MET C1 C2	12	13	29.4 ± 2.0	11.7 ± 0.9	34.3 ± 2.1	−6.1 ± 2.3
	MET_C03	29	6	52.7 ± 1.4	12.4 ± 0.6	37.8 ± 1.5	−7.3 ± 1.6
	MET_C05	14	10	56.8 ± 1.4	−0.4 ± 0.6	16.8 ± 1.5	−9.2 ± 1.6
	MET_D04	25	7	52.2 ± 1.4	16.4 ± 0.6	39.8 ± 1.5	−4.3 ± 1.6
	MET_F01	14	5	54.3 ± 1.4	19.3 ± 3.5	44.4 ± 1.9	−3.8 ± 4.0
	MET_F02	13	6	48.5 ± 1.4	7.8 ± 3.5	24.3 ± 1.9	−4.8 ± 4.0
	MET_E03	20	6	34.6 ± 1.4	15.7 ± 3.6	41.5 ± 1.9	−5.9 ± 4.0
	MET_F03	12	5	41.9 ± 1.4	20.6 ± 3.6	45.9 ± 1.9	−3.3 ± 4.0
	MET_F04	24	6	36.2 ± 1.4	19.0 ± 3.6	42.7 ± 1.9	−3.2 ± 4.0
	MET_G01	24	6	32.9 ± 1.4	11.6 ± 3.3	36.7 ± 1.3	−7.5 ± 3.6
	MET_G04	22	5	43.4 ± 2.0	22.9 ± 3.3	49.4 ± 3.8	−2.8 ± 5.1
	MET_G05	16	6	42.8 ± 2.0	23.6 ± 3.3	45.7 ± 3.8	−0.2 ± 5.1
	MET_H02	18	11	39.0 ± 2.0	21.1 ± 3.3	45.3 ± 3.8	−2.4 ± 5.1
	MET_H03	33	8	34.6 ± 2.0	21.5 ± 3.3	40.3 ± 3.8	0.5 ± 5.1
	MET_H04	19	7	39.8 ± 2.0	25.0 ± 3.3	41.9 ± 3.8	3.2 ± 5.1
	MET_B03	10	8	52.9 ± 0.5	4.1 ± 1.4	19.8 ± 1.5	−6.2 ± 2.0
	MET_B01	7	8	36.0 ± 0.5	15.3 ± 1.4	40.5 ± 1.5	−5.8 ± 2.0
	MET_B04	24	6	37.2 ± 0.5	11.7 ± 1.4	33.7 ± 1.5	−5.8 ± 2.0
	MET_C04	22	5	33.1 ± 1.4	15.1 ± 0.6	36.8 ± 1.5	−4.0 ± 1.6
Dolomite						
	META6			53.3 ± 1.0	7.2 ± 0.2	9.5 ± 0.7	2.3 ± 1.3
	META7			55.5 ± 1.1	5.7 ± 0.2	17.0 ± 0.7	−3.2 ± 1.3
	META17			51.0 ± 1.0	12.4 ± 0.2	22.2 ± 0.7	0.8 ± 1.3
	META19			42.4 ± 1.1	0.3 ± 0.2	17.1 ± 0.7	−8.6 ± 1.3

*All errors are 2-sigma uncertainty.
CL spectral signatures are in counts/second.

The other group has relatively high $\delta^{13}C$ and low $\delta^{18}O$ values and consists of Mn-rich calcite from MET 01070 and dolomite from all three samples.

Again, there are no significant changes to the results when possible bias from matrix-effects are considered (see Section 2.4 for details). The $\delta^{13}C$ values do not

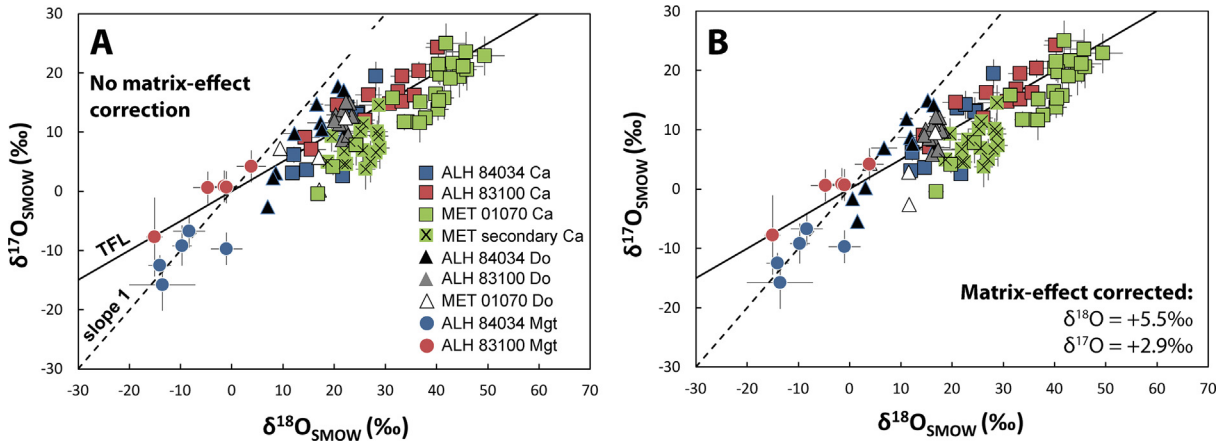

Fig. 6. Three O-isotope plots for individual calcite (Ca, squares), dolomite (Do, triangles), and magnetite (Mgt, circles) grains from MET 01070, ALH 83100, and ALH 84034. The uncertainties are 2σ. Matrix-effects have been evaluated (see Section 2.4 for details). Both matrix-uncorrected (A) and -corrected (B) data are shown for comparison (only the dolomite values change).

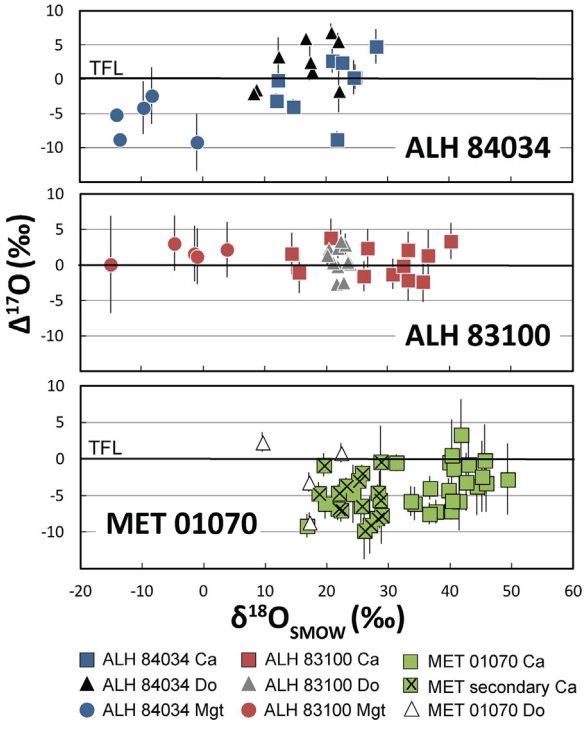

Fig. 7. The $\Delta^{17}O$ values for calcite (squares), dolomite (triangle), and magnetite (crosses) from MET 01070, ALH 83100, and ALH 84034. Error bars are 2σ.

change significantly. The $\delta^{18}O$ values of shift to the left on the $\delta^{13}C$ vs. $\delta^{18}O$ plot. The matrix-corrected data are shown in Fig. 6B and 8B, but are not discussed any further.

4. DISCUSSION

There is ample evidence that most carbonates in CM chondrites are extra-terrestrial in origin. Nevertheless, it is important to bear in mind that carbonate formation and/or modification could occur during a meteorite's terrestrial residence (Velbel et al., 1991; Tyra et al., 2007). The weathering grades for ALH 83100, ALH 84034 and MET 01070 are Be, A, and Be, respectively (https://www.lpi.usra.edu/meteor/metbull.php). Tyra et al. (2007) found evidence for a terrestrial carbonate component in addition to extraterrestrial carbonate from bulk $\delta^{18}O$, $\delta^{13}C$ and the fraction of modern day ^{14}C of Antarctic CM chondrites similar to those analyzed for this study. However, *in situ* $\delta^{18}O$ analyses of carbonate from the same samples found that most carbonate grains had extraterrestrial $\delta^{18}O$ compositions, except a carbonate vein (Tyra et al., 2012). These studies indicate that the terrestrial component occurs as veins or as fine-grained material not easily analyzed with SIMS. Veins were not observed in ALH 83100 or ALH 84034. At least one thin carbonate vein was observed in MET 01070, but it was too small and not analyzed. MET 01070 also contained areas in the matrix consisting of large patches of fine-grained mixtures of dolomite and calcite. These materials were too fine-grained to be analyzed by SIMS. Carbonate ages determined from ^{53}Mn-^{53}Cr dating provide some of the best support for the pre-terrestrial origin of carbonates in CM chondrites (de Leuw et al., 2009; Fujiya et al., 2012; Lee et al., 2012; Jilly et al., 2014). Excess ^{53}Cr in carbonates from ALH 83100 indicate they formed within a few million years after CAIs (Fujiya et al., 2012). Here, we assume that carbonates in ALH 84034 and MET 01070 are also pre-terrestrial in origin, although their ages have not been determined. This is supported by similar bulk carbonate $\delta^{13}C$ and $\delta^{18}O$ values for CM falls and finds (Alexander et al., 2015).

4.1. Petrology

Calcite grains in all three CM chondrites analyzed for this study are predominantly type 1 euhedual to subhedral grains with few if any mineral inclusions. These are thought to have formed as precipitates from melting of pore ices

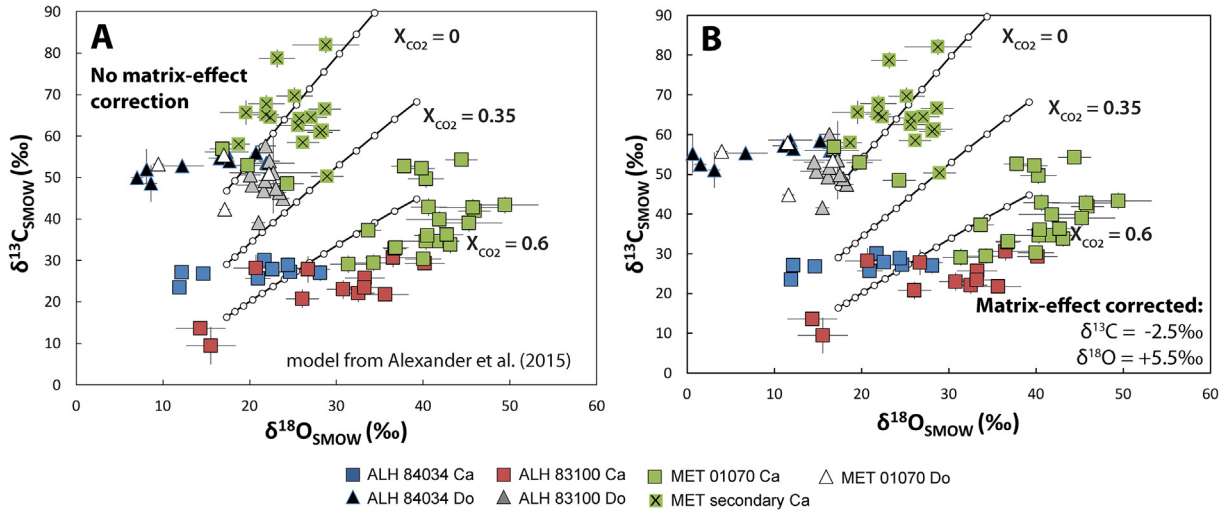

Fig. 8. The $\delta^{13}C$ vs. $\delta^{18}O$ for calcite (squares) and dolomite (triangles) in MET 01070, ALH 83100, and ALH 84034. The uncertainties are 2σ. The data are compared to models in which calcite crystallizes at various temperatures (between 0 °C and 130 °C, from right to left) from an aqueous fluid that is in equilibrium with a CO (or CH_4) and CO_2 gas mixture (Alexander et al., 2015). Models are represented by the lines on the figure. Matrix-effects have been evaluated (see Section 2.4 for details). Both matrix-uncorrected (A) and -corrected (B) C and O isotope data are shown for comparison (only the dolomite values change).

(Lee et al., 2014) and, if correct, must be the first carbonates to form. Mottled (or type 2) calcite grains have been observed in various CM chondrites and are thought to be secondary (Tyra et al., 2013; Lee et al., 2014). We only observed a few type 2 grains in MET 01070 and none in the ALH samples. We classify Mn-rich calcite in MET 01070 as secondary based on the CL signatures (described in Section 3.2). They are not mottled like type 2 grains described by Tyra et al. (2007; 2012, 2013) and Lee et al. (2014). Variations in CL signatures of calcite similar to those describe in Section 3.2 have been observed in other CM chondrites (Lee and Ellen, 2008; Brearley and Hutcheon, 2002) and were attributed to variations in Mn concentration during carbonate crystallization within an open pore. However, we do not think this is the case for secondary calcite in MET 01070, instead it likely represents a distinct calcite formation event.

We observe two petrologic types of dolomite grains. One type is spatially associated with calcite, often with calcite occurring as inclusions within the dolomite grains (Fig. 9A and B). There is a second type that appears to be pseudomorphic replacements of phyllosilicates (Fig. 9C and D). The occurrence of these different petrologic types of calcite and dolomite are indications of either episodic carbonate precipitation, probably related to the dissolution and re-precipitation of earlier formed carbonate, or highly localized variations in the fluid composition during carbonate formation. Lee et al. (2014) argue for early dolomite formation based on predicted variations in the Mg/Ca ratio of the evolving fluid and based on the occurrence of intergrowths between Ca carbonate and phyllosilicates. However, in MET 01070, dolomite grains are associated with Mn-rich calcite, which we argue is secondary based on its occurrence on the periphery of euhedral Mn-poor calcite grains (see Fig. 5). Secondary formation of Mn-rich calcite is also supported by its slightly lower $\Delta^{17}O$ values compared to Mn-poor calcite (Fig. 7). The petrographic and O-isotopic data indicates that dolomite in MET 01070 formed after primary (Mn-poor) calcite precipitation and formed contemporaneously with or after the secondary (Mn-rich) calcite. Since dolomite grains in all three samples have relatively similar $\delta^{13}C$ and $\delta^{18}O$ values (Fig. 8A), they may have all formed under similar conditions, likely as a result of dissolution and reprecipitation reactions in the parent body. Thus, primary (Mn-poor) calcite likely provides the best constraints on initial aqueous alteration conditions while dolomite and secondary (Mn-rich) calcite record secondary processes.

4.2. Non-equilibrium conditions of carbonate formation in CM chondrites

The C and O isotopic composition of Ca-carbonates in the three CM1 thin sections analyzed for this study span larger ranges than the bulk analyses of 64 CM chondrites reported by Alexander et al. (2015). The homogeneous $\Delta^{17}O$ values of ALH 83100 indicate that the carbonates in this sample formed from fluid that had equilibrated with the rock, while the variation in the $\Delta^{17}O$ values for ALH 84034 and MET 01070 indicate that the O isotopic composition of the fluid changed during carbonate formation as a result of continued fluid-rock interaction.

The $\delta^{13}C$ and $\delta^{18}O$ fractionation factors can potentially be used to place constraints on the conditions of carbonate formation in the parent body. Equilibrium C and O isotope fractionation should result in differences between dolomite and calcite of no more than 5‰ and 3‰, respectively (Sheppard and Schwarcz, 1970; Kim and O'Neil, 1997). However, we observe dolomite-calcite $\delta^{13}C$ fractionation of 26‰ ± 6‰ for ALH 84034 and 26‰ ± 16‰ for ALH 83100 (2SD). For MET 01070, $\delta^{13}C_{dol\text{-}cal}$ is −14‰ ± 19‰ for secondary calcite and 9‰ ± 21‰ for primary calcite

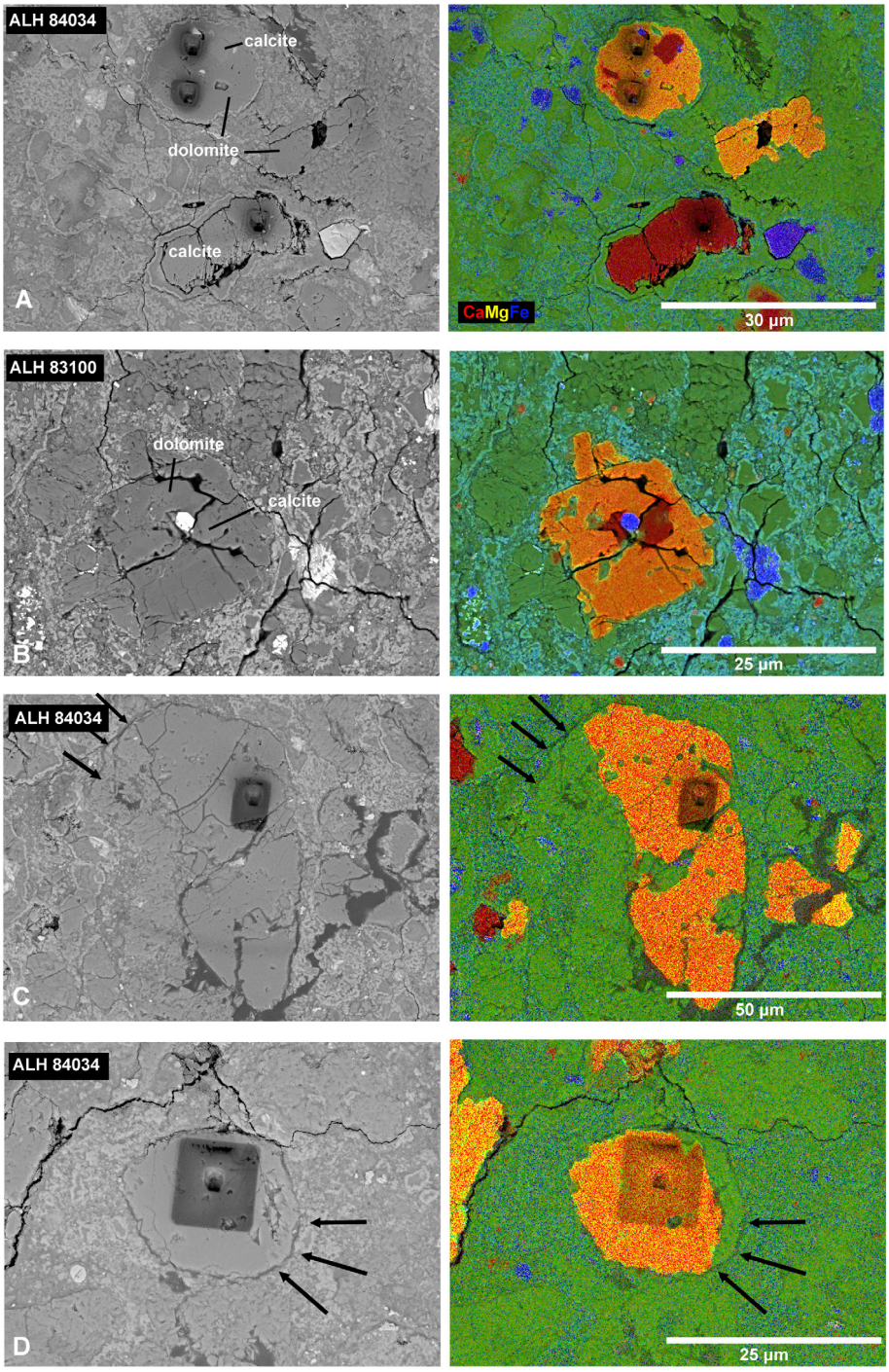

Fig. 9. BSE and false color images of calcite (red) and dolomite (yellow-orange) in ALH 84034 and ALH 83100. There are two main types of dolomite in these samples, those that are spatially associated with calcite (a and b), and those that are associated with pseudomorphic replacement phyllosilicates (c and d). Arrows highlight the grain boundary of phyllosilicate that was partially replaced by dolomite. (For interpretation of the references to color in this figure legend, the reader is referred to the web version of this article.)

(2SD). These values are derived from subtracting the average of the $\delta^{13}C$ values for calcite and dolomite. Dolomite-calcite $\delta^{18}O$ isotope fractionation values are all negative, again, inconsistent with equilibrium conditions. Non-equilibrium $\delta^{13}C_{dol\text{-}cal}$ and $\delta^{18}O_{dol\text{-}cal}$ values persist even when only calcite and dolomite grains that are in close proximity (within 200 microns) are considered.

The dolomite grains analyzed in all three meteorites have similar $\delta^{13}C$ values, 49‰ ± 10‰ for ALH 83100, 53‰ ± 5‰ for ALH 84034, and 51‰ ± 11‰ for MET

01070 (2SD). There is a range of ~25‰ in $\delta^{18}O$ for dolomite grains in ALH 84034 that appears to correlate with the petrologic type of dolomite (Fig. 8A and 9). Dolomite associated with calcite tends to be depleted in $\delta^{18}O$ (average of two analyses is ~8‰) compared to those associated with pseudomorphic phyllosilicate replacement (average of six analyses is ~17‰). The two different types of dolomite either: (1) formed at different times and at different temperatures, or (2) formed at the same time, but the differences in the $\delta^{18}O$ values partly reflect the composition of the material that they replaced (i.e., calcite versus phyllosilicates). The latter scenario is consistent with the similar ^{53}Mn-^{53}Cr ages of calcite and dolomite (Fujiya et al., 2012) and also consistent with the $\delta^{18}O$ composition of the CM matrix, which predominately consists of phyllosilicates (Clayton et al., 1999). Further petrographic and isotopic analyses are necessary to better constrain the formation of these two types of dolomite.

4.3. Temperature constraint from dolomite-magnetite isotope fractionation in ALH 83100

We measured the O-isotopic composition of magnetite in ALH 83100 and ALH 84034. Under equilibrium conditions, the dolomite-magnetite or calcite-magnetite $\delta^{18}O$ fractionation could potentially place constraints on the temperatures of their formation (Zheng et al., 1994; Kim and O'Neil, 1997). The $\Delta^{17}O$ values of two phases that formed in equilibrium should be the same, but this is not observed for carbonate and magnetite in ALH 84034 (Fig. 7). Therefore, both the $\delta^{18}O_{Ca\text{-}Mgt}$ and $\delta^{18}O_{Do\text{-}Mgt}$ values for this sample do not provide reliable temperature constraints. The dolomite-magnetite $\delta^{18}O$ fractionation of ALH 83100 provides our best constraint. Calcite, dolomite and magnetite in ALH 83100 fall on a single mass fractionation line (Fig. 7). Calcite grains in this sample exhibit large variations in $\delta^{18}O$ values (14–40‰), indicating that the assumption of equilibrium for calcite may not be appropriate. Dolomite has a more limited range in $\delta^{18}O$ values (20–23‰), suggesting more equilibrium conditions for dolomite formation. If we only consider single isolated magnetite grains in ALH 83100 (all except 'mgt 1'), there is a range in $\delta^{18}O$ values of ~8‰, an average magnetite $\delta^{18}O$ composition of $-0.8‰ \pm 7‰$ (2SD) and a corresponding $\delta^{18}O_{Do\text{-}Mgt}$ value of $23‰ \pm 7‰$ (2SD). Though it is not clear whether magnetite and dolomite formed in equilibrium, this fractionation implies temperatures of $125\ °C \pm 60\ °C$ (2SD) for dolomite and magnetite formation in ALH 83100 (Fig. 10). This is consistent with estimates from clumped isotope thermometry of carbonates from CMs (20–71 °C; Guo and Eiler, 2007), tochinilite stability (<120 °C; Zolensky et al., 1993), and geochemical modeling (0–200 °C from Schulte and Shock, 2004 and 0–130 °C from Alexander et al., 2015; 110 °C; Verdier-Paoletti et al., 2017).

4.4. Comparison of calcite from CM1s and CM2s

In Fig. 11, we compare our analyses to previous *in situ* studies of calcite and dolomite (Tyra et al., 2012; Lee

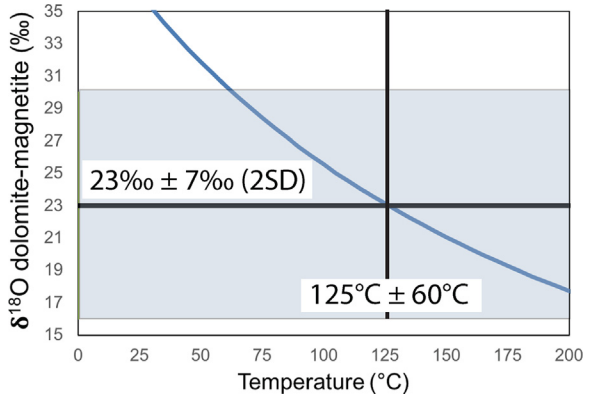

Fig. 10. The variation in equilibrium dolomite-magnetite $\delta^{18}O$ fractionation as a function of temperature (blue solid line) based on the work of Zheng et al. (1994) and Kim and O'Neil (1997). The crosshairs show the estimated formation temperature of dolomite and magnetite based on the $\delta^{18}O_{dol\text{-}mgt}$ fractionation in ALH 83100 (excluding the framboidal magnetite grain mgt1). (For interpretation of the references to color in this figure legend, the reader is referred to the web version of this article.)

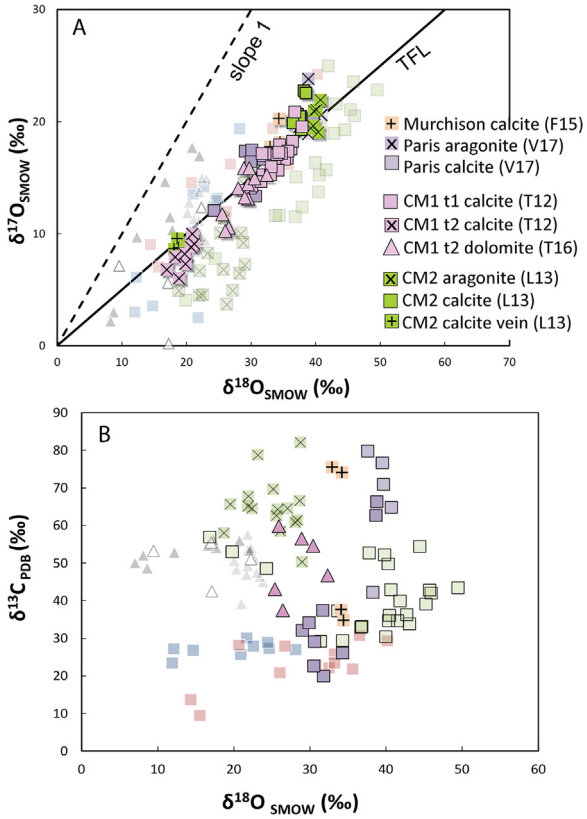

Fig. 11. Comparison of previous *in situ* analyses to this study. (a) O-isotopic compositions of carbonate grains analyzed in previous data legend: F15: Fujiya et al. (2015); V17: Vacher et al. (2017); T16: Tyra et al. (2016); L13: Lee et al. (2013). (b) C and O isotope analyses from previous *in situ* analyses. These figures are similar to Figs. 6 and 8. Refer to those figures for the complete legend and see text for discussion of petrologic type classification.

et al., 2013; Fujiya et al., 2015; Vacher et al., 2017). To reiterate, we classify the samples according to the scheme proposed by Alexander et al. (2013) in which the petrologic type is a linear function of the degree of hydration and the scale varies from 1.0 to 2.9. In this scheme, most CMs have petrologic types that are less than 2.0 (i.e., more than 50% of their originally anhydrous minerals have been altered). By contrast, in the classification scheme of Rubin et al. (2007), the most altered CMs have a petrologic type of 2.0 and the least altered would be 2.9. In this case, there is no traditional CM1. While there is a general correlation between the classification schemes of Rubin et al. (2007) and Alexander et al. (2013), there is also considerable scatter. This scatter is presumably due to the inherent uncertainties in both schemes, as well as heterogeneity in the meteorites themselves. Thus, at present there is some confusion in the literature about CM petrologic classification. For example, Tyra et al. (2012) refer to samples EET 96006, EET 96016, EET 96017, and EET 96019 as CM2s, but these are described as a CM 1.3 in Alexander et al. (2013). Therefore in Fig. 11, the data from Tyra is classified as CM1. Lee et al. (2013) describes LON 94101 as a CM 2.2–2.3 following Rubin et al. (2007), while Alexander et al. (2013) classifies it as CM 1.8. In Fig. 11, it is classified as a CM2.

The range in the O isotope composition of carbonates from this study shows more variation, but is consistent with previous analyses of CM1 and CM2 chondrites (Fig. 11A). Data for MET 01070 has a large spread in $\delta^{18}O$ values compared to the others and the reason for this is unclear. Calcite in ALH 83100 and primary calcite in MET 01070 are isotopically similar to type 1 calcite and aragonite in CM1 and CM2 chondrites, suggesting that they all precipitated from similar fluid compositions or under similar conditions. However, CM1 carbonates have many grains that are depleted in $\delta^{18}O$ compared to CM2s, which may indicate longer duration of water rock interaction. The O isotopic composition for type 2 calcite from Tyra et al. (2012) and a calcite vein from Lee et al. (2013) are similar to secondary calcite in MET 01070 and calcite in ALH 84034, again suggesting formation under similar fluid conditions. The $\delta^{18}O$ of dolomite from this study are not consistent with those from the CM1 ALH 84049 (Tyra et al., 2016), while the $\delta^{13}C$ values of dolomite are consistent (Fig. 11B). Similar to CM1 carbonates, calcite in CM2s appear to have two groups based on their $\delta^{13}C$ values. Altogether, the C and O isotopic data indicates that the fluid composition and aqueous alteration conditions for carbonate formation in CM1s and CM2s were initially similar, but CM1s likely experienced longer duration of aqueous alteration.

4.5. Source of C and constraints on the conditions of carbonate growth

Presolar grains and organic matter are potential sources of C for carbonate formation. They exhibit a wide range of $\delta^{13}C$ values (Amari et al., 2014), but the abundances of presolar grains in CMs are low (Leitner et al., 2015) and most of the C-rich presolar grains (SiC, graphite, and diamond) are fairly resistant to low temperature alteration. The $\delta^{13}C$ of −15‰ for insoluble organic matter in CM chondrites is inconsistent with the carbonate compositions (Alexander et al., 1998). The range of $\delta^{13}C$ values for water-soluble organic compounds in CMs (0–65‰) are comparable to those of carbonates in CMs; however, the abundances of this material are quite low, up to ~100 nmol/g in CM chondrites (Aponte et al., 2016). When compared to the 0.3 wt.% C in carbonates, presolar grains and water-soluble organics cannot be the predominate reservoir of C for carbonate formation.

Volatile C species trapped in ices that were accreted by the CM parent body are a more likely C source for carbonates. In comets, CO, CO_2, and CH_4 are the dominant C-bearing volatile species (e.g., Mumma and Charnley, 2011; Ootsubo et al., 2012). While cometary ices probably formed at significantly lower temperatures than the CM chondrites, ices that formed in the interstellar medium or in the colder regions of the outer Solar System and then were transported inwards would be able to retain some of their volatiles even as temperatures approached the sublimation temperature of water-ice (e.g., Mousis et al., 2008).

Alexander et al. (2015) analyzed the bulk carbonate compositions in 64 CMs. They found a similar but somewhat more restricted range of bulk carbonate C and O isotopic compositions to those observed for the *in situ* data presented here (Fig. 8A). A model of carbonate precipitation from a single aqueous fluid in equilibrium with a gas that was dominated by CH_4 and/or CO at temperatures from 0 to 130 °C predicts a positive correlation between $\delta^{13}C$ and $\delta^{18}O$ that can reproduce most but not all of the bulk data. They find that varying the fraction of CO_2 in the gas can explain the full range of the bulk data.

In Fig. 9, we compare the *in situ* data to the carbonate precipitation models from Alexander et al. (2015). Primary (Mn-poor) calcite from all three samples fall near the trend for high CO_2 fractions (>60%), while secondary (Mn-rich) calcite from MET and dolomite from all three samples fall near the model trend for low CO_2 fractions (<10%). This would require that the conditions of the fluid changed from oxidizing to reducing during aqueous alteration. This model assumes constant fluid and gas isotopic compositions (i.e., effectively infinite fluid reservoirs) during carbonate formation, which is unlikely. The large range in $\Delta^{17}O$ values for ALH 84034 and MET 01070 carbonates show that the fluid compositions did vary due to interaction with anhydrous minerals. Hence, the sizes and compositions of the fluid and/or gas reservoirs likely changed with progressive alteration and precipitation of carbonates. Guo and Eiler (2007) carried out clumped-isotope analyses of $\delta^{13}C$ and $\delta^{18}O$ of carbonates in three CM falls (Cold Bokkeveld, Murray, and Murchison), but found a negative correlation between $\delta^{13}C_{carbonate}$ and $\delta^{18}O_{water}$. They explain the $\delta^{13}C$ variation of carbonates in CMs with escape of CH_4 enriched in ^{12}C during Rayleigh-type isotopic fractionation processes. The negative correlation reported by Guo and Eiler (2007), but not seen by Alexander et al. (2015), is based on results from only three meteorites, and thus could be a statistical fluke, but, the low $\delta^{13}C$ values of primary calcite and high $\delta^{13}C$ values of secondary calcite in MET 01070 could potentially be consistent with this model as well.

Nevertheless, the cathodoluminescence signatures of primary (Mn-poor) and secondary (Mn-rich) calcite in MET 01070 (Fig. 5) are consistent with oxidizing and reducing conditions, respectively, as indicated by the Alexander et al. (2015) model (Barnaby and Rimstidt, 1989). Also, a fluid composition that is initially oxidizing and then becomes more reducing is consistent with geochemical models of progressive aqueous alteration in the CM chondrite parent body (Schulte and Shock, 2004). The variation in temperature from 0 to 130 °C inferred from the Alexander et al. (2015) model is consistent with the temperature estimated from dolomite-magnetite O isotope fractionation in ALH 83100. The large temperature variations on a thin-section scale could be a result of multiple stages of dissolution and reprecipitation, where some fraction of the carbonate grains survive each episode of dissolution (Lindgren et al., 2012). Multi-stage carbonate growth has been inferred from several previous studies (e.g., Brearley, 2006, de Leuw et al., 2010, Lee et al., 2014, Tyra et al., 2016). Additional work is needed to constrain what processes controlled dissolution and reprecipitation of carbonates in the CM parent body (e.g., convective fluid flow (e.g., Young et al., 1999)? or impact processing (e.g., Lindegren et al., 2011)?).

5. SUMMARY AND CONCLUSIONS

We measured *in situ* the C and O isotopic compositions of individual calcite and dolomite grains, and the O isotopic compositions of magnetite grains from the highly altered CM chondrites ALH 83100, ALH 84034, and MET 01070 in order to constrain the conditions that led to their extensive aqueous alteration in the CM parent body. Petrographic and cathodoluminescence observations of calcite in MET 01070 provide clear indications of multiple generations of calcite formation. Mn-rich calcite grains are anhedral and often occur along the periphery of euhedral/subhedral Mn-poor calcite grains. We have characterized the Mn-rich and Mn-poor calcite grains in MET 01070 as secondary and primary calcite, respectively. This relationship is supported by the slightly lower $\Delta^{17}O$ values of Mn-rich calcite compared to Mn-poor calcite, which is expected if Mn-rich calcite formed from a more evolved fluid.

Calcite and dolomite grains from these three CM1s exhibit large variations in their C and O isotopic compositions that span the entire range of values exhibited by bulk analyses of 64 CM chondrites (Alexander et al., 2015). The data fall into two groups on a $\delta^{13}C$ vs. $\delta^{18}O$ plot: one group consists of primary (Mn-poor) calcite from all three samples, it has relatively low $\delta^{13}C$ (10–60‰) and high $\delta^{18}O$ (10–50‰) values, while the other group consists of secondary (Mn-rich) calcite from MET 01070 and dolomite from all three samples and has relatively high $\delta^{13}C$ (40–80‰) and low $\delta^{18}O$ (10–30‰) values. Dolomite in MET 01070 occurs with secondary (Mn-rich) calcite. Since dolomite grains in all three samples have similar $\delta^{13}C$ and $\delta^{18}O$ values (40–50‰ for $\delta^{13}C$ and 10–20‰ for $\delta^{18}O$), they may have all formed under similar conditions following primary (Mn-poor) calcite formation.

Overall, our results suggest that: (1) primary (Mn-poor) calcite, characterized by depleted $\delta^{13}C$ and enriched $\delta^{18}O$ values, provides a more pristine record of the initial fluid composition and aqueous alteration conditions compared to secondary (Mn-rich) calcite and dolomite that tend to be enriched in ^{13}C and depleted in ^{18}O, (2) the fluid composition and the carbonate formation conditions were initially similar for both CM1s and CM2s based on the significant overlap in their carbonate isotopic compositions, but primary calcite in CM1s extend to lower $\delta^{18}O$ values, possibly indicating a longer duration of alteration, (3) dolomite formation in ALH 83100 occurred at temperatures of 125 °C ± 60 °C (2SD), which is consistent with previous estimates of carbonate formation, (4) the range of carbonate $\delta^{13}C$ and $\delta^{18}O$ values can be explained if they precipitated from a fluid in equilibrium with CO (or CH_4) and varying proportions of CO_2 as proposed by Alexander et al. (2015); though Rayleigh fractionation associated with preferential loss of ^{12}C-depleted CH_4 (Guo and Eiler, 2007) could not be ruled out and (5) the large isotopic variations on the thin-section scale may be due to multiple episodes of partial dissolution-reprecipitation reactions in the parent body.

ACKNOWLEDGEMENTS

The authors acknowledge associate editor Rhian Jones and three anonymous reviewers for their helpful comments. Many thanks to E. Bullock for assistance with electron probe analyses. Thanks also to K.D. McKeegan (UCLA), and J.G. Wynn (USF) for the terrestrial standards. US Antarctic meteorite samples are recovered by the Antarctic Search for Meteorites (ANSMET) program, which has been funded by NSF and NASA, and characterized and curated by the Department of Mineral Sciences of the Smithsonian Institution and Astromaterials Curation Office at NASA Johnson Space Center.

APPENDIX A. SUPPLEMENTARY MATERIAL

Supplementary data to this article can be found online at https://doi.org/10.1016/j.gca.2019.06.012.

REFERENCES

Alexander C. M. O'D., Russell S. S., Arden J. W., Ash R. D., Grady M. M. and Pillinger C. T. (exander et al. 1998) The origin of chondritic macromolecular organic matter: a carbon and nitrogen isotope study. *Meteorit. Planet. Sci.* **33**, 603–622.

Alexander C. M. O'D., Howard K., Bowden R. and Fogel M. L. (2013) The classification of CM and CR chondrites using bulk H, C and N abundances and isotopic compositions. *Geochim. Cosmochim. Acta* **123**, 244–260.

Alexander C. M. O'D., Bowden R., Fogel M. L. and Howard K. T. (2015) Carbonate abundances and isotopic compositions in chondrites. *Meteorit. Planet. Sci.* **50**, 810–833.

Amari S., Zinner E. and Gallino R. (2014) Presolar graphite from the Murchison meteorite: an isotopic study. *Geochim. Cosmochim. Acta* **133**, 479–522.

Aponte J. C., McLain H. L., Dworkin J. P. and Elsila J. E. (2016) Aliphatic amines in Antarctic CR2, CM2, and CM1/2 carbonaceous chondrites. *Geochim. Cosmochim. Acta* **189**, 296–311.

Barnaby R. J. and Rimstidt J. D. (1989) Redox conditions of calcite cementation interpreted from Mn and Fe contents of authigenic calcites. *Geol. Soc. Am. Bull.* **101**, 795–804.

Benedix G. K., Leshin L. A., Farquhar J., Jackson T. and Thiemens M. H. (2003) Carbonates in CM2 chondrites: constraints on alteration conditions from oxygen isotopic compositions and petrographic observations. *Geochim. Cosmochim. Acta* **67**, 1577–1588.

Boggs S. and Krinsley D. (2006) Application of Cathodoluminescence Imaging to the Study of Sedimentary Rocks. Cambridge University Press, UK.

Brearley A. J. and Hutcheon I. D. (2000) Carbonates in the CM1 chondrite ALH84034: Mineral chemistry, zoning and Mn-Cr systematics. *Lunar Planet. Sci.* **XXXI**, 1407.pdf.

Brearley A. J. and Hutcheon I. D. (2002) Carbonates in the Y79119 CM2 chondrite: zoning and Mn-Cr systematics. *Meteorit. Planet. Sci.* **37**, A23.

Brearley A. J. (2006) The role of microchemical environments in the alteration of CM carbonaceous chondrites. *Lunar Planet. Sci. 37th Annual Lunar and Planetary Science Conference, March 13-17, 2006, League City, Texas*, abstract no. 2074.

Clayton R. N. and Mayeda T. K. (1984) The oxygen isotope record in Murchison and other carbonaceous chondrites. *Earth Planet. Sci. Lett.* **67**, 151–161.

Clayton R. N. and Mayeda T. K. (1999) Oxygen isotope studies of carbonaceous chondrites. *Geochim. Cosmochim. Acta* **63**, 2089–2104.

de Leuw S., Rubin A. E., Schmitt A. K. and Wasson J. T. (2009) ^{53}Mn-^{53}Cr systematics of carbonates in CM chondrites: implications for the timing and duration of aqueous alteration. *Geochim. Cosmochim. Acta* **73**, 7433–7442.

de Leuw S., Rubin A. E. and Wasson J. T. (2010) Carbonates in CM chondrites: Complex formational histories and comparison to carbonates in CI chondrites. *Meteorit. Planet. Sci.* **45**, 513–530.

Fujiya W., Sugiura N., Hotta H., Ichimura K. and Sano Y. (2012) Evidence for the late formation of hydrous asteroids from young meteoritic carbonates. *Nat. Commun.* **3**, 627.

Fujiya W., Sugiura N., Marrocchi Y., Takahata N., Hoppe P., Shirai K., Sano Y. and Hiyagon H. (2015) Comprehensive study of carbon and oxygen isotopic compositions, trace element abundances, and cathodoluminescence intensities of calcite in the Murchison CM chondrite. *Geochim. Cosmochim. Acta* **161**, 101–117.

Grady M. M., Wright I. P., Swart P. K. and Pillinger C. T. (1988) The carbon and oxygen isotopic composition of meteoritic carbonates. *Geochim. Cosmochim. Acta* **52**, 2855–2866.

Guo W. and Eiler J. M. (2007) Temperatures of aqueous alteration and evidence for methane generation on the parent bodies of the CM chondrites. *Geochim. Cosmochim. Acta* **71**, 5565–5575.

Howard K. T., Alexander C. M. O. D., Schrader D. L. and Dyl K. A. (2015) Classification of hydrous meteorites (CR, CM and C2 ungrouped) by phyllosilicate fraction: PSD-XRD modal mineralogy and planetesimal environments. *Geochim. Cosmochim. Acta* **149**, 206–222.

Jarosewich E. and MacIntyre I. G. (1983) Carbonate reference samples for electron microprobe and scanning electron microscope analyses. *J. Sediment. Petrol.* **52**, 677–678.

Jilly C. E., Huss G. R., Krot A. N., Nagashima K., Yin Q.-Z. and Sugiura N. (2014) ^{53}Mn-^{53}Cr dating of aqueously formed carbonates in the CM2 lithology of the Sutter's Mill carbonaceous chondrite. *Meteorit. Planet. Sci.* **49**, 2104–2117.

Kim S.-T. and O'Neil J. R. (1997) Equilibrium and nonequilibrium oxygen isotope effects in synthetic carbonates. *Geochim. Cosmochim. Acta* **61**, 3461–3475.

King A. J., Schofield P. F. and Russell S. S. (2017) Type 1 aqueous alteration in CM carbonaceous chondrites: implications for the evolution of water-rich asteroids. *Meteorit. Planet. Sci.* **52**, 1197–1215.

Kita N. T., Ushikubo T., Fu B. and Valley J. W. (2009) High precision SIMS oxygen isotope analysis and the effect of sample topography. *Chem. Geol.* **264**, 43–57.

Lee M. R. and Ellen R. (2008) Aragonite in Murray (CM2) carbonaceous chondrite: implications for parent body compaction and aqueous alteration. *Meteorit. Planet. Sci.* **43**, 1219–1231.

Lee M. R., Lindgren P., Sofe M. R., Alexander C. M. O. D. and Wang J. (2012) Extended chronologies of aqueous alteration in the CM2 carbonaceous chondrites: Evidence from carbonates in Queen Alexandra Range 93005. *Geochimica et Cosmochimica Acta* **92**, 148–169. https://doi.org/10.1016/j.gca.2012.06.005.

Lee M. R., Sofe M. R., Lindgren P., Starkey N. A. and Franchi I. A. (2013) The oxygen isotope evolution of parent body aqueous solutions as recorded by multiple carbonate generations in the Lonewolf Nunataks 94101 CM2 carbonaceous chondrite. *Geochim. Cosmochim. Acta* **121**, 452–466.

Lee M. R., Lindgren P. and Sofe M. R. (2014) Aragonite, breunnerite, calcite and dolomite in the CM carbonaceous chondrites: High fidelity recorders of progressive parent body aqueous alteration. *Geochim. Cosmochim. Acta* **144**, 126–156.

Leitner L., Hoppe P., Metzler K., Haenecour P., Floss C. and Vollmer C. (2015) The presolar grain inventory of CM chondrites. *Meteorit. Planet. Sci. 78th Annual Meeting of the Meteoritical Society, held July 27–31, 2015 in Berkeley, California*, LPI Contribution No. 1856, p. 5178.

Lindgren P., Lee M. R. and Sofe M. (2012) Evidence for multiple fluid pulses in the CM1 carbonaceous chondrite parent body. *Lunar Planet. Sci. 43rd Lunar and Planetary Science Conference, held March 19–23, 2012 at The Woodlands, Texas*, LPI Contribution No. 1659, p. 1949.

Lindgren P., Lee M. R., Sofe M. and Burchell M. J. (2011) Microstructure of calcite in the CM2 carbonaceous chondrite LON 94101: implications for deformation history during and/or after aqueous alteration. *Earth Planet. Sci. Lett.* **306**, 289–298.

Mousis O., Alibert Y., Hestroffer D., Marboeuf U., Dumas C., Carry B., Horner J. and Selsis F. (2008) Origin of volatiles in the main belt. *Mon. Not. R. Astron. Soc.* **383**, 1269–1280.

Mumma M. J. and Charnley S. B. (2011) The chemical composition of comets – emerging taxonomies and natal heritage. *Annu. Rev. Astron. Astrophys.* **49**, 471–524.

Ootsubo T., Kawakita H., Hamada S., Kobayashi H., Yamaguchi M., Usui F., Nakagawa T., Ueno M., Ishiguro M., Sekiguchi T., Watanabe J.-I., Sakon I., Shimonishi T. and Onaka T. (2012) AKARI Near-infrared spectroscopic survey for CO_2 in 18 Comets. *Astrophys. J.* **752**, 15.

Richter D. K., Gotte Th., Gotze J. and Neuser R. D. (2003) Progress in application of cathodoluminescence (CL) in sedimentary petrology. *Mineral. Petrol.* **79**, 127–166.

Rollion-Bard C. and Marin-Carbonne J. (2011) Determination of SIMS matrix effects on oxygen isotopic compositions in carbonates. *J. Anal. Atomic Spec.* **26**, 1285–1289.

Rubin A. E., Trigo-Rodriguez J. M., Huber H. and Wasson J. T. (2007) Progressive aqueous alteration of CM carbonaceous chondrites. *Geochim. Cosmochim. Acta* **71**, 2361–2382.

Schulte M. and Shock E. (2004) Coupled organic synthesis and mineral alteration on meteorite parent bodies. *Meteorit. Planet. Sci.* **39**, 1577–1590.

Sheppard S. M. F. and Schwarcz H. P. (1970) Fractionation of carbon and oxygen isotopes and magnesium between coexisting metamorphic calcite and dolomite. *Contrib. Mineral. Petrol.* **26**, 161–198.

Sliwinski M. G., Kitajima K., Kozdon R., Spicuzza M. J., Fournelle J. H., Denny A. and Valley J. W. (2015a) Secondary ion mass spectrometry bias on isotope ratios in Dolomite-Ankerite, Part II: $\delta^{13}C$ matrix effects. *Geostand. Geoanal. Res.* **40**, 173–184.

Sliwinski M. G., Kitajima K., Spicuzza M. J., Orland I. J., Ishida A., Fournelle J. H. and Valley J. W. (2015b) Secondary ion mass spectrometry bias on isotope ratios in Dolomite-Ankerite, Part III: $\delta^{18}O$ matrix effects. *Geostand. Geoanal. Res.* **42**, 49–76.

Tyra M. A., Farquhar J., Wing B. A., Benedix G. K., Jull A. J. T., Jackson T. and Thiemens M. H. (2007) Terrestrial alteration of carbonate in a suite of Antarctic CM chondrites: evidence from oxygen and carbon isotopes. *Geochim. Cosmochim. Acta* **71**, 782–795.

Tyra M. A., Farquhar J., Guan Y. and Leshin L. A. (2012) An oxygen isotope dichotomy in CM2 chondritic carbonates – a SIMS approach. *Geochim. Cosmochim. Acta* **77**, 383–395.

Tyra M., Brearley A. and Guan Y. (2016) Episodic carbonate precipitation in the CM chondrite ALH 84049: An ion microprobe analysis of O and C isotopes. *Geochim. Cosmochim. Acta* **175**, 195–207.

Vacher L. G., Marrocchi Y., Villeneuve J., Verdier-Paoletti M. J. and Gounelle M. (2017) Petrographic and C & O isotopic characteristics of the earliest stages of aqueous alteration of CM chondrites. *Geochim. Cosmochim. Acta* **213**, 271–290.

van Schmus W. R. and Wood J. A. (1967) A chemical-petrologic classification for the chondritic meteorites. *Geochim. Cosmochim. Acta* **31**, 747–765.

Velbel M. A., Long D. T. and Gooding J. L. (1991) Terrestrial weathering of Antarctic stone meteorites: formation of Mg-carbonates on ordinary chondrites. *Geochim. Cosmochim. Acta* **55**, 67–76.

Verdier-Paolettia M. J., Marrocchi Y., Avice G., Roskosz M., Gurenko A. and Gounelle M. (2017) Oxygen isotope constraints on the alteration temperatures of CM chondrites. *Earth Planet. Sci. Lett.* **458**, 273–281.

Young E. D., Ash R. D., England P. and Rumble, III, D. (1999) Fluid flow in chondritic parent bodies: deciphering the compositions of planetesimals. *Science* **286**, 1331–1335.

Zheng Y.-F. (1994) Oxygen isotope fractionation in magnetites: structural effect and oxygen inheritance. *Chem. Geol.* **121**, 309–316.

Zolensky M., Barrett R. and Browning L. (1993) Mineralogy and composition of matrix and chondrule rims in carbonaceous chondrites. *Geochim. Cosmochim. Acta* **57**, 3123–3148.

Zolensky M. E., Mittlefehldt D. W., Lipschutz M. E., Wang M.-S., Clayton R. N., Mayeda T. K. and Barber D. J. (1997) CM chondrites exhibit the complete petrologic range from type 2 to 1. *Geochim. Cosmochim. Acta* **61**, 5099–5115.

Associate editor: Rhian Jones